# Performance of UWB $N$-Orthogonal PPM in AWGN and Multipath Channels

Fernando Ramírez-Mireles, *Senior Member, IEEE*

***Abstract*—This paper studies pulse-based $M$-ary ultrawideband communications analyzing both the symbol error rate (SER) and the information theoretic capacity $C$ for single-link communications over both additive white Gaussian noise and multipath channels (taking into account random variations in both energy and correlation values). In particular, we consider $M$-ary $N$-orthogonal pulse-position-modulated (PPM) signals with numerical pulse-position optimization to exploit the negative values in the pulse correlation function. On one hand, the $N$-orthogonal PPM ($N$-OPPM) signals can accommodate a larger value of $M$ than the nonoverlapping orthogonal PPM (OPPM) signals for a constant frame size and pulse width, allowing increasing the symbol transmission rate and/or the use of error correcting codes. However, $N$-OPPM requires a receiver with $N$ correlators, while the receiver for OPPM requires one correlator. On the other hand, the pulse positions of the $N$-OPPM signals can be manipulated to shape the power spectrum density and decrease the level of the discrete components. However, this PPM manipulation changes the $N$-OPPM correlation properties of the signal set. At the same time, $N$-OPPM signals have equal or better performance than OPPM signals. More specifically, simulations show that for low values of $M$, the $N$-OPPM has lower SER and higher $C$ than OPPM for the same signal-to-noise ratio (SNR), and that for larger values of $M$, it achieves similar SER and $C$. Hence, $N$-OPPM signals allow a tradeoff between transmission rate, signal performance, and receiver complexity.**

***Index Terms*—Block waveform signal design, channel capacity, multipath channels, pulse-position modulation (PPM), ultrawideband (UWB), UWB communications.**

## I. Introduction

PULSE-BASED ultrawideband (UWB) communications have been the subject of intense research activity recently [1]–[6]. The use of $M$-ary pulse-position modulation (PPM), pulse amplitude modulation (PAM), and other $M$-ary modulation schemes allows to increase the number of users supported by the system for a given data transmission rate without degrading the multiple access performance. More importantly, for UWB communications, $M$-ary signals allow to reduce the required transmitter power maintaining the number of users, the data transmission rate, and the multiple access performance [7]–[15].

This paper studies the performance of pulse-based UWB $M$-ary $N$-orthogonal PPM (OPPM) signals. We analyze both the symbol error rate (SER) and the capacity $C$ for a single-link[1] UWB communications over both the additive white Gaussian noise (AWGN) and multipath channels. This paper is organized as follows. In Section II, we provide a motivation to use the $N$-OPPM signals. In Section III, we describe the structure of the $N$-OPPM signals and calculate the corresponding power spectrum density (PSD). Section IV describes the system model used for SER and $C$ calculations. In Section V, we address the signal optimization. In Section VI, we calculate the SER. In Section VII, we compute $C$. Sections VIII–X include numerical examples of signal design and PSD, SER, and $C$, respectively. Section XI contains a discussion of results and conclusions.

## II. Motivation to Use $N$-OPPM Signals

The $M$-ary PPM signals have been widely used in optical communications. This signaling scheme generally changes the position of the light intensity with respect to a frame sync. Hence, previous results in $M$-ary PPM signal design, from simple orthogonal signals to designs based on the algebraic constructions such as [18]–[20], could be considered for UWB $M$-ary communications signal sets. However, most of these previous PPM signal designs presume that pulses are not overlapping and do not take advantage of the negative correlation properties of the pulses used in UWB wireless communications.

The motivation of this paper is the design of $M$-ary PPM communications signals that can provided a performance enhancement as $M$ grows avoiding an $M$-fold increase in the complexity of the receiver. Hence, we are looking for signal designs that allow a tradeoff between transmission rate, SER performance and receiver complexity (number of correlators).

In this paper, we study the $N$-orthogonal signals,[2] which is a generalization of biorthogonal signals. An $N$-orthogonal-signal set consists of $M = NL$ signals, where $M$, $N$, and $L$ are all

Manuscript received April 26, 2004; revised June 13, 2005, May 31, 2006, and June 5, 2006. This work was presented in part in (F. Ramírez-Mireles, "UWB $M$-ary $N$-Orthogonal PPM Signals in AWGN and Multipath Channels," in *Proc. IEEE Veh. Technol. Conf.,* pp. 5255–5259, Oct. 2004) and (F. Ramírez-Mireles, "Capacity of UWB $M$-ary 2-Orthogonal PPM Signals in AWGN and Multipath Channels," in *Proc. IEEE 39th Annual Asilomar Conference on Signals, Systems, and Comput.,* Nov. 2005). The review of this paper was coordinated by Prof. R. Qiu.

The author is with the Digital Systems Department, Instituto Tecnológico Autónomo de México, México City, D.F. C.P. 01000, México (e-mail: ramirezm@ieee.org).

Color versions of one or more of the figures in this paper are available online at http://ieeexplore.ieee.org.

Digital Object Identifier 10.1109/TVT.2007.895488

[1]Multiple access performance of $N$-OPPM signals over free-space propagation conditions was studied in [8].

[2]The $N$-orthogonal phase-modulated signals were first introduced by Reed and Scholtz [22] and later studied by Viterbi and Stiffler [23]. The $N$-orthogonal pulse-position-modulated signals were introduced in [24].

Fig. 1. (a) $N$-OPPM signals with $N = 4$, $L = 4$ can accommodate $M = 16$ signals in $T_f$ ns. (b) OPPM signals can accommodate $M = 6$ signals in the same $T_f$ ns. Example with pulse duration $T_w = 2$ ns, $T_o = 2.76$ ns, and frame time $T_f = 12$ ns.

integers greater than zero. The $M$ equal energy and equal time duration signals have the following two properties.

1) The signal set may be divided into $L$ disjoint subsets, each subset containing $N$-correlated (e.g., nonorthogonal) members.
2) Signals from different subsets are orthogonal.

Hence, this class of signals can be contained in $L$-orthogonal subspaces, and $N$-correlated signals are packed in each subspace. In particular, the PPM-based 2-OPPM signals (i.e., $N = 2$) are analogous to the PAM-based biorthogonal signals.[3] One important difference is that PPM signals cannot be antipodals (if signals were antipodals, that would mean that there exists a time shift such that the shifted signal is equal to its negative for all time, which is not possible). Hence, an $M$-ary biorthogonal set is formed by $M/2$ orthogonal signals and their $M/2$ antipodals, but a 2-OPPM set is formed by $M/2$ orthogonal signals and their $M/2$ quasi-antipodals.

We notice that $N$-OPPM signals can accommodate a larger value of $M$ than the OPPM signals for a constant frame size $T_f$ and pulse width $T_w$. More specifically, for OPPM, $M \leq \lfloor T_f/T_w \rfloor$, and for $N$-OPPM, $M \leq N\lfloor T_f/T_o \rfloor$, where $T_o$ is the time shift separating orthogonal subsets, and $\lfloor \cdot \rfloor$ denotes the integer part. As an example, Fig. 1 shows a case where $M = 16$ for $N$-OPPM and $M = 6$ for OPPM.

By increasing $M$, $N$-OPPM allows to increase the symbol transmission rate and/or the use of error correcting codes. For the example in Fig. 1, the maximum bit transmission rate $R_b$ for $N$-OPPM is $\log_2(16)/\log_2(6) \simeq 1.6$ larger than the $R_b$ for OPPM. In this same example, $N$-OPPM can be combined with a forward error correcting code with rate 2/3 and still have the same $R_b$ transmission rate at the line than using OPPM. We must note, however, that $N$-OPPM requires a receiver with $N$ correlators, while the receiver for OPPM requires one correlator.[4]

At the same time, we are interested in the $N$-OPPM signals that have equal or better performance than the OPPM signals. For this purpose, we perform a numerical pulse-position optimization to exploit the negative values in the pulse correlation function. With this optimization, we can get better performance for low values of $M$. However, we must remember that in AWGN channels, the signal-to-noise-ratio (SNR) gain that is obtained by using negatively correlated $M$-ary signals to improve SER decreases as $M$ increases [21]. Hence, for higher values of $M$, performance of $N$-OPPM and OPPM should be similar.

Finally, we mention that we can exploit the $M$-ary PPM-modulation parameters to shape the PSD of the $N$-OPPM signals.

## III. $N$-OPPM Signals and Their PSD

Under free-space propagation conditions, the $N$-OPPM signals are denoted [24]

$$\Psi_{n,l}(t) = \sum_{k=0}^{N_s-1} \sqrt{E_{\rm a}} w(t - kT_f - \tau_n + lT_o) \qquad (1)$$

where $t$ denotes time, $n = 1, 2, \ldots, N$, $l = 0, 1, 2, \ldots, L-1$, $N$, $L$ are both positive nonzero integers. The time-shift values $\tau_1 = 0,\ \tau_1 < \tau_2 \leq T_w, \ldots, \tau_{N-1} < \tau_N \leq (N-1)T_w,\ T_o \triangleq T_w + \tau_N$, and $T_f$ is the frame repetition period. The $w(t)$ is the UWB pulse used to construct the PPM signals and has duration $T_w$ and average energy $E_{\rm a}$. In (1), we use the double index $(n, l)$ instead of a single index $i = lN + n$, $i = 1, 2, \ldots, M$ to emphasize that the signals $\Psi_{n,l}(t)$ with different values of $l$ belong to different orthogonal subsets.

Under multipath conditions (e.g., a slowly varying indoor radio channel, where the transmitter is placed at a certain fixed location, and the receiver is placed at a variable location denoted $u_o$), the $M$-ary PPM signals containing the multipath effects can be denoted

$$\Psi_{n,l}(u_o, t) = \sum_{k=0}^{N_s-1} \sqrt{E_{\rm a}} w(u_o, t - kT_f - \tau_n + lT_o) \qquad (2)$$

where the "pulse" $\sqrt{E_{\rm a}} w(u_o, t)$ is a multipath spread version of $\sqrt{E_{\rm a}} w(t)$ received at position $u_o$ with average duration $T_{\rm a} \gg T_w$ and "random" energy $E_w(u_o) \triangleq E_{\rm a}\beta^2(u_o)$, where

$$\beta^2(u_o) \triangleq \int_{-\infty}^{\infty} [w(u_o, t)]^2\, dt.$$

[3]The $M$-ary biorthogonal signals have the desirable property that they can achieve the same or better SER than orthogonal signals using receivers with half the complexity than orthogonal signals [21].

[4]There are also $N$-OPPM signals that require only two correlators for any value of $N$ [8].

The signals in (1) have duration $T_s = N_s T_f$, where $T_f > T_w + LT_o$, with pulse duration $T_w$. The signals in (2) have duration $T_s = N_s T_f$, where $T_f > T_{\rm a} + LT_o$, with "pulse" duration $T_{\rm a}$. We use the same $\tau_n,\ n = 1, 2, \ldots, N$, and $T_o = T_w + \tau_N$ for both the free-space and multipath cases. The condition on $T_f$ ensures that we can ignore interpulse and intersymbol interference.

Next, we define energy and correlation values for the multipath case in (2). For the free-space channel case in (1), we just drop the index $u_o$ and use $\beta^2(u_o) = 1$.

The signals $\Psi_{n,l}(u_o, t)$ in (2) have "random" energy

$$E_\Psi(u_o) = \int_{-\infty}^{\infty} \left[\Psi_{n,l}(u_o, \xi)\right]^2 d\xi \simeq \overline{E}_\Psi \beta^2(u_o) \tag{3}$$

where $\overline{E}_\Psi = N_s E_{\rm a}$ is the average signal energy. The signals $\Psi_{n_1,l_1}(u_o, t)$ and $\Psi_{n_2,l_2}(u_o, t)$ have "random" normalized correlation values

$$\begin{aligned}\alpha(u_o) &\triangleq \alpha_{n_1,n_2,l_1,l_2}(u_o)\\ &= \frac{\int_{-\infty}^{\infty} \Psi_{n_1,l_1}(u_o,\xi)\Psi_{n_2,l_2}(u_o,\xi)d\xi}{E_\Psi(u_o)}.\end{aligned}$$

Because "pulses" in different frames are nonoverlapping, the $N$-OPPM signals will have correlation matrix $\Gamma_{\rm NO}(u_o) \triangleq [\alpha(u_o)]_{M\times M}$ with elements

$$\alpha(u_o) = \begin{cases} 0, & \text{if } l_1 \neq l_2 \\ & \text{(different subsets)} \\ 1, & \text{if } l_1 = l_2, n_1 = n_2 \\ & \text{(correlation with itself)} \\ \gamma(u_o, \tau_{n_2} - \tau_{n_1}), & \text{if } l_1 = l_2, n_1 \neq n_2 \\ & \text{(same subset)} \end{cases} \tag{4}$$

where

$$\gamma(u_o, \tau) \triangleq \frac{\int_{-\infty}^{\infty} \sqrt{E_{\rm a}} w(u_o, t) \sqrt{E_{\rm a}} w(u_o, t-\tau) dt}{\int_{-\infty}^{\infty} \left[\sqrt{E_{\rm a}} w(u_o, t)\right]^2 dt} \tag{5}$$

is the normalized signal correlation function of $\sqrt{E_{\rm a}} w(u_o, t)$, with $\gamma(u_o, \tau) > -1\ \forall \tau$.

For the signals in (1), we define $\tau_{\min}$ as the value of $\tau$ such that $\gamma(\tau)$ attains its minimum value $\gamma_{\min}$, i.e., $\gamma_{\min} \triangleq \gamma(\tau_{\min})$. For the signals in (2), we use the same $\tau_{\min}$; hence, $\gamma_{\min}(u_o) \triangleq \gamma(u_o, \tau_{\min})$.

Using (1) with $N = 1$, $L = M$, we can define the $M$-ary OPPM signals having diagonal correlation matrix $\Gamma_{\rm OR}$. Another way to define OPPM is by using $L = 1$, $N = M$ with time shifts $\tau_i = (n-1)T_w$, $n = 1, 2, \ldots, N$.

### A. PSD of $M$-ary $N$-OPPM Signals

Using the time-averaged PSD defined in [25], the PSD of the ensemble of signals in (1) can be shown to be

$$\begin{aligned}\text{PSD}(f) = \frac{1}{T_s}\Bigg\{ &\sum_{i=1}^{M} P_i(1-P_i)\left|F_{\Psi_i}(f)\right|^2 - \\ &2\sum_{\substack{i=1\\ i\neq j}}^{M}\sum_{\substack{j=1\\ i<j}}^{M} P_i P_j \mathcal{R}\left\{F_{\Psi_i}(f) F^*_{\Psi_j}(f)\right\} + \\ &\frac{1}{T_s^2}\sum_{m=-\infty}^{\infty}\left|\sum_{i=1}^{M} P_i F_{\Psi_i}\left(\frac{m}{T_s}\right)\right|^2 \delta\left(f - \frac{m}{T_s}\right)\Bigg\}\end{aligned}$$

$$\triangleq \frac{\left|F_w(f)\right|^2}{T_s}\left\{\text{PSD}_c(f) + \text{PSD}_d(f)\sum_{m=-\infty}^{\infty}\frac{1}{T_s}\delta\left(f - \frac{m}{T_s}\right)\right\} \tag{6}$$

where

$$\begin{aligned} j &\triangleq l_1 N + n_1, \qquad j = 1, 2, \ldots, M \\ &\text{for} \quad n_1 = 1, 2, \ldots, N, \qquad l_1 = 0, 1, 2, \ldots, L-1 \\ i &\triangleq l_2 N + n_2, \qquad i = 1, 2, \ldots, M \\ &\text{for} \quad n_2 = 1, 2, \ldots, N, \qquad l_2 = 0, 1, 2, \ldots, L-1 \end{aligned}$$

and where $f$ is the frequency in hertz, $[|F_w(f)|^2/T_s]\text{PSD}_c(f)$ is the magnitude of the continuous component of $\text{PSD}(f)$, $[|F_w(f)|^2/T_s^2]\text{PSD}_d(f)$ is the magnitude of the discrete component of $\text{PSD}(f)$, $\delta(f)$ is the Dirac delta function, $(\cdot)^*$ denotes the complex conjugate operator, $\mathcal{R}\{\cdot\}$ denotes the real value operator, $P_i$ is the probability of signal $\Psi_i(t)$ being used, $F_{\Psi_i}(f) = F_w(f)\ F_i(f)$ is the Fourier transform of $\Psi_i(t)$, $F_w(f)$ is the Fourier transform of $w(t)$, and where

$$\begin{aligned}F_{i=lN+n}(f) = \exp[-j2\pi(\tau_n + lT_o)f] \\ \times \sum_{k=0}^{N_s-1}\exp[-jk(2\pi T_f)f]\,.\end{aligned} \tag{7}$$

Notice that for $P_i = 1/M$, we have

$$\begin{aligned}\sum_{i=lN+n}^{M} P_i \exp[-j2\pi(\tau_n + lT_o)f] \\ = \frac{1}{M}\sum_{l=0}^{L-1}\exp[-jl(2\pi T_o)f]\sum_{n=1}^{N}\exp[-j(2\pi\tau_n)f]\,.\end{aligned} \tag{8}$$

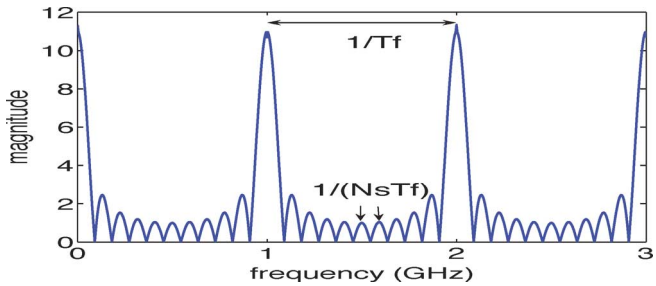


Fig. 2. Plot for $|(\sin[N_s(2\pi T_f)(f/2)])/(\sin[(2\pi T_f)(f/2)])|$ for $N_s = 11$ and $T_f = 10$ ns.

Also, notice that [26]

$$\sum_{k=0}^{N_s-1} \exp[-jk(2\pi T_f)f] = \exp\left[-j\frac{N_s-1}{2}(2\pi T_f)f\right] \frac{\sin[N_s(2\pi T_f)f/2]}{\sin[(2\pi T_f)f/2]}. \quad (9)$$

Fig. 2 shows a plot of the magnitude of (9).

Using (6)–(9), we can write

$$\text{PSD}_d(f) = \left|\frac{\sin[N_s(2\pi T_f)f/2]}{\sin[(2\pi T_f)f/2]}\right|^2 \left|\frac{\sin[L(2\pi T_o)f/2]}{\sin[(2\pi T_o)f/2]}\right|^2 \times \frac{1}{M^2}\left|\sum_{n=1}^{N}\exp[-j(2\pi\tau_n)f]\right|^2 \quad (10)$$

and

$$\text{PSD}_c(f) = \left|\frac{\sin[N_s(2\pi T_f)f/2]}{\sin[(2\pi T_f)f/2]}\right|^2 \times \left[\frac{M-1}{M} - \frac{2}{M^2}\sum_{\substack{i=l_1N+n_1\\ i\neq j}}^{M}\sum_{\substack{j=l_2N+n_2\\ i<j}}^{M} \times \cos\left(2\pi\left(\tau_{n_1}-\tau_{n_2}+(l_1-l_2)T_o\right)f\right)\right] \quad (11)$$

As expected, the final PSD in (6) is a function of the pulse shape (factor $|F_w(f)|$) and the $M$-ary PPM-modulation parameters [factors $\text{PSD}_c(f)$ and $\text{PSD}_d(f)$]. If, besides the PPM modulation, a time-hopping (TH) spread-spectrum modulation is introduced in $\Psi_i(t)$ in the same fashion as in [1] and [8], the effects will be to simultaneously spread and reduce the PSD level.[5]

[5]When the received is synchronized, introducing a TH modulation does not change the correlation properties in (4). When the pseudorandom TH sequence has periodicity $N_s$, then we can still use the PSD in (6) with a different $F_i(f)$ in (7) because in every symbol interval, we are transmitting with the same set of TH–PPM signals.

Fig. 3. (a) Model to calculate SER in continuous time AWGN. (b) Model for calculation of SER in multipath channels. (c) Equivalent vector channel model used to calculate $C$ in both AWGN and multipath channels.

## IV. System Model

Fig. 3 illustrates the models used to calculate SER and $C$.

### A. System Model for the AWGN Channel

Fig. 3(a) shows this model. On the transmitter side, we consider an $M$-ary $N$-OPPM modulator with an input vector $\overline{U}$ and an output signal $\Psi_{\text{TX}}(t)$. The vector $\overline{U} = (u_1, u_2, \ldots, u_k)$ is the output of a $k$-bit source, where $M = 2^k$, with all $\overline{U}$ being equally likely.

Under free-space propagation conditions, the received signal $\Psi(t)$ is modeled as the derivative of the transmitted signal $\Psi_{\text{TX}}$ [1][6] that is modified by amplitude $A_o$ and delay $\tau_o$ factors that depend on the transmitter–receiver separation distance $D$. In our analysis, we will assume $A_o = 1$ and $\tau_o = 0$. The $n(t)$ is AWGN with two-sided PSD $N_o/2$.

For the receiver, we consider time-shift-coherent communications. For decoding, we use the $M$-ary correlation receiver with perfect synchronization [21]. To detect the $M$ signals, we need to correlate the input signal with $M$ reference signals. Let $y(t)$ be the received signal that is composed of one of the signals in (1) plus AWGN. Each one of the receiver's $M = NL$ channel correlation outputs can be written

$$d_{i=lN+n} = \int_0^{N_sT_f} y(t)\Psi_{n,l}(t)dt = \sum_{k=0}^{N_s-1}\sum_{q=0}^{L-1}\delta_{q,l}z_n(k,q)$$

[6]This model for the antenna system has been repeatedly used [1]–[5]. Most existing UWB antennas do not have the differentiation effect. Even for these antennas, the results in this paper can still be applied, since the analysis is based on the energy and correlation values of the received signals.

TABLE I
EXAMPLE WITH VALUES OF $\overline{U}$ AND $\overline{\Psi}$ FOR $k = 3$, $M = 8 = NL$, $N = 2$, AND $L = 4$. THE INDEX $i = l \cdot N + n$

| $(l, n, i)$ | $\overline{U}$ | $\overline{\Psi}$ |
|---|---|---|
| (0,1,1) | (0,0,0) | $\sqrt{E_\Psi}\left(+\psi^{(+)},+\psi^{(-)},0,0,0,0,0,0\right)$ |
| (0,2,2) | (0,0,1) | $\sqrt{E_\Psi}\left(+\psi^{(+)},-\psi^{(-)},0,0,0,0,0,0\right)$ |
| (1,1,3) | (0,1,0) | $\sqrt{E_\Psi}\left(0,0,+\psi^{(+)},+\psi^{(-)},0,0,0,0\right)$ |
| (1,2,4) | (0,1,1) | $\sqrt{E_\Psi}\left(0,0,+\psi^{(+)},-\psi^{(-)},0,0,0,0\right)$ |
| (2,1,5) | (1,0,0) | $\sqrt{E_\Psi}\left(0,0,0,0,+\psi^{(+)},+\psi^{(-)},0,0\right)$ |
| (2,2,6) | (1,0,1) | $\sqrt{E_\Psi}\left(0,0,0,0,+\psi^{(+)},-\psi^{(-)},0,0\right)$ |
| (3,1,7) | (1,1,0) | $\sqrt{E_\Psi}\left(0,0,0,0,0,0,+\psi^{(+)},+\psi^{(-)}\right)$ |
| (3,2,8) | (1,1,1) | $\sqrt{E_\Psi}\left(0,0,0,0,0,0,+\psi^{(+)},-\psi^{(-)}\right)$ |

where

$$z_n(k,q) \triangleq \int_{kT_f+qT_o}^{kT_f+(q+1)T_o} y(t)w(t - kT_f - \tau_n - qT_o)dt$$

is the output of one of the $N$ correlators operating simultaneously, and $\delta_{q,q'}$ is the Kronecker delta. From the expression for $d_i$, it is clear that the receiver needs only $N$ correlation and $M = NL$ store and sum circuits. The $d_i$ can be calculated while $y(t)$ is received, and no symbol delay occurs.

### B. System Model for the Multipath Channel

Fig. 3(b) shows this model. On the transmitter side, we have the same modulator and transmitted signals as in the AWGN case. Under multipath conditions, the received signal is $\Psi(u_o, t)$. In our analysis, we consider the received signal as a whole random process, with no differentiation between the multipath components.

For the receiver, we consider again the time-shift-coherent communications. For decoding, we use a kind of Rake receiver [27] ideally matched to the received signals and perfectly synchronized with the transmitter.

### C. Vector Model for Capacity Calculations

To simplify the notation, the vector model and the capacity calculation will correspond to the AWGN channel. To find the model and results for the multipath case, we just add an index $u_o$ to each expression to denote that those quantities are conditioned to a certain location $u_o$.

The vector model that will be used for capacity calculation is shown in Fig. 3(c). This model is valid for 2-OPPM, i.e., for $N = 2$ and $M = 2L$, with $\tau_1 = 0$ and $\tau_2 = \tau$, having $M/2$ orthogonal subsets with two signals in each subset, where

$$\alpha = \begin{cases} 0, & \text{if } l_1 \neq l_2 \\ 1, & \text{if } l_1 = l_2, n_1 = n_2 \\ \gamma(\tau), & \text{if } l_1 = l_2, n_1 \neq n_2. \end{cases} \quad (12)$$

We consider an $M$-ary 2-OPPM modulator with equally likely input $\overline{U}$ and output $\overline{\Psi}$. The $M$-dimensional vector $\overline{\Psi} = \sqrt{E_\Psi}(\psi_1, \psi_2, \ldots, \psi_M)$ represents one of the $M$-ary 2-OPPM signals $\Psi_{n,l}(t)$. These communication vectors are the projections of the received signals with respect to an orthonormal basis whose elements are

$$\Phi_{1l}(t) \triangleq \frac{\Psi_{1l}(t) + \Psi_{2l}(t)}{2\sqrt{E_\Psi}\psi^{(+)}} \quad \text{and} \quad \Phi_{2l}(t) \triangleq \frac{\Psi_{1l}(t) - \Psi_{2l}(t)}{2\sqrt{E_\Psi}\psi^{(-)}}$$

where

$$\psi^{(+)} \triangleq \sqrt{\frac{1+\gamma(\tau)}{2}} \quad \text{and} \quad \psi^{(-)} \triangleq \sqrt{\frac{1-\gamma(\tau)}{2}}.$$

However, in the multipath case, the vector model is valid only for the case $N = 2$ with $L = 1$, i.e., $M = 2$ signals.[7]

An example with vectors $\overline{U}$ and $\overline{\Psi}$ for $M = 8$ is shown in Table I. The vector construction in Table I can be generalized for any valid $L$. The reader can verify that the vectors $\overline{\Psi}_{n,l}$ in Table I all have energy $E_\Psi$, and that any pair of vectors $\overline{\Psi}_{n_1,l_1}$ and $\overline{\Psi}_{n_2,l_2}$ have normalized correlation values $\alpha$ in (12).

The vector $\overline{\Psi}$ is sent through the AWGN channel in Fig. 3(c). The output of the channels is $\overline{Y} = \overline{\Psi} + \overline{W}$, where $\overline{Y} = (y_1, y_2, \ldots, y_M)$, and $\overline{W} = (\varrho_1, \varrho_2, \ldots, \varrho_M)$ is a real AWGN noise vector with zero mean and variance $\sigma^2 = N_o/2$ in each dimension.[8]

## V. SIGNAL OPTIMIZATION

### A. Previous Results for AWGN

The optimal signal-design problem (OSDP) for coherent communications in AWGN was previously studied in [28] and [29]. The work in [28] expresses the error probability $P_e$

[7] In the presence of multipath, the signal orthogonality for different $L$ is destroyed [30]. Hence, this vector model is appropriate to model the random variations of energy and correlation values for two signals.

[8] Capacity is calculated at the output of the channel. The matched filters are included to illustrate how energy and correlation of received signals are calculated.

as a function of the SNR, the signal correlation matrix $\Lambda = [\lambda_{n_1 n_2}]_{N\times N}$, the number of signals in the $N$-ary set, and the dimensionality of the signal set $D$.[9] The work in [29] uses the union bound on error probability $\mathrm{UB}_e$, which is clearly a function of the SNR, $\Lambda$, $N$, and $D$.

The solution to the OSDP is to determine the optimum signal sets with the best $\Lambda$ that minimizes $P_e$ or $\mathrm{UB}_e$ for various $N$ and $D$, determining the dependence or independence of these optimal sets from the SNR.[10] In the general case, the solution is to be found in a signal space conformed by:

1) $N$ equal-energy equally probable signals;
2) No constraints on $D$, other than $D \leq N$;
3) No constraints on $\Lambda$, other than it must be a valid correlation matrix, i.e., it must satisfy the following.
   a) $\Lambda = \Lambda^\top$ (i.e., $\Lambda$ is equal to its transpose).
   b) $\mathbf{X}\Lambda\mathbf{X}^\top \geq 0$, for all $\mathbf{X} \in \Re^N$, where $\Re$ is the set of real numbers.
   c) $\lambda_{n_1 n_1} = 1, n_1 = 1, 2, \ldots, N$.
   d) $-1 \leq \lambda_{n_1 n_2} \leq 1, n_1 \neq n_2, n_1, n_2 = 1, 2, \ldots, N$.

In this paper, we use the linearly independent PPM signals (i.e., $D = N$) with the extra constraint $-1 < \gamma_{\min} \leq \lambda_{n_1 n_2} = \gamma(\tau_{n_2} - \tau_{n_1}) \leq 1$, for $n_1 \neq n_2$, $n_1, n_2 = 1, 2, \ldots, N$. Hence, previous work in OSDP is not restricted to a particular correlation function, whereas in this paper, the signal design is constrained to a given signal correlation function.

### B. Previous Results for Multipath

The work in [30] formulates the signal design for binary PPM UWB communications taking into consideration the particular characteristics of UWB propagation in a dense multipath channel. Within the context of [30], signal design is the process to find information signals that have "good distance" properties and, therefore, provide good bit-error-rate performance [28]. In this signal design, the squared distance depends on a time-shift parameter $\tau$. Hence, the BER also depends on $\tau$. The results show that, in general, the UWB signal design that is best suited for the AWGN channel is different from the UWB signal design that is best suited for the multipath channel. In this paper, we do not optimize the $N$-OPPM signals in multipath channels.

### C. $N$-OPPM Signal Optimization in AWGN

For UWB pulses, the $\gamma(\tau)$ in (5) has negative values; hence, we can find negatively correlated signals by choosing the appropriate values of time shifts

$$\Omega_N \triangleq (\tau_1, \tau_2, \ldots, \tau_N). \tag{13}$$

As we have seen, the negatively correlated signals reduce SER in AWGN channels [28], [29].

[9]As an example, both $M$-ary phase-shift keying and quadrature-amplitude modulation have $D = 2$, and biorthogonal, simplex, and orthogonal have $D = M/2$, $D = M - 1$, and $D = M$, respectively.

[10]For both $P_e$ or $\mathrm{UB}_e$, the solution to the OSDP is the optimum signal set known as the regular simplex set [28], [29] with $D = N - 1$ and $\lambda_{n_1 n_2} \triangleq (-1/N - 1), n_1 \neq n_2$.

This paper describes the three *ad hoc* signal-optimization criteria to reduce the SER. For this purpose, notice that we just need to find the $N$ negatively correlated signals inside each of the $L$-orthogonal subsets. Also, notice that we can write

$$\Gamma_{\mathrm{NO}} = \begin{bmatrix} \Lambda(\Omega_N) & \mathbf{O} & \ldots & \mathbf{O} \\ \mathbf{O} & \Lambda(\Omega_N) & \ldots & \mathbf{O} \\ \vdots & \vdots & \ddots & \vdots \\ \mathbf{O} & \mathbf{O} & \ldots & \Lambda(\Omega_N) \end{bmatrix}_{NL\times NL}$$

where $\Lambda(\Omega_N) \triangleq [\lambda_{n_1 n_2}]_{N\times N}$ is the correlation matrix of the $N$ signals belonging to any of the $L$ subsets, with

$$\lambda_{n_1 n_2} = \begin{cases} 1, & n_1 = n_2 \\ \gamma(\tau_{n_2} - \tau_{n_1}), & n_1 \neq n_2 \end{cases}$$

$n_1, n_2 = 1, 2, \ldots, N$.

Notice that $\Lambda(\Omega_N)$ is also the correlation matrix of the set of signals

$$w(t - \tau_1), w(t - \tau_2), \ldots, w(t - \tau_N).$$

Hence, the optimization problem is reduced from a set with $M$ signals to a set with $N$ signals. The three signal-optimization criteria are as follows.

1) Find the $\Omega_N$ that minimizes the SER for shift-coherent communications in the presence of AWGN [28]

$$P_e\left(\frac{E_\mathrm{a}}{N_o}, \Lambda(\Omega_N)\right) = 1 - \frac{1}{N}\exp\left(\frac{1}{2}\frac{E_\mathrm{a}}{N_o}\right)\Phi\left(\sqrt{\frac{E_\mathrm{a}}{N_o}}, \Lambda(\Omega_N)\right)$$

where $\Phi(\sqrt{E_\mathrm{a}/N_o}, \Lambda(\Omega_N)) = E_{\mathbf{W}}\{\exp(\sqrt{E_\mathrm{a}/N_o}\max_i \varrho_i)\}$, $\mathbf{W}$ is an $N$-dimensional Gaussian random vector with probability density function (pdf) $\mathcal{N}(\mathbf{0}, \Lambda(\Omega_N))$, $\varrho_i$, $i = 1, 2, \ldots, N$ are the elements of $\mathbf{W}$, $(E_\mathrm{a}/N_o)$ is the SNR, and $E_{\mathbf{W}}\{\cdot\}$ is the expected value operator.

2) Calculate the $\Omega_N$ that minimizes the union bound on the SER

$$\mathrm{UB}_e\left(\frac{E_\mathrm{a}}{N_o}, \Lambda(\Omega_N)\right) = \frac{1}{N}\sum_{\substack{n_1=1 \\ n_1\neq n_2}}^{N}\sum_{n_2=1}^{N} Q\left(\sqrt{\frac{E_\mathrm{a}}{N_o}(1 - \gamma(\tau_{n_2} - \tau_{n_1}))}\right)$$

where $Q(\cdot)$ is the Gaussian tail integral.

3) Find $\Omega_{\rm N}$ that solves the optimization problem

$$\begin{aligned}\underset{\text{all possible } \Omega_N}{\text{minimize}} \quad & \max\big(\gamma(\tau_{12}),\gamma(\tau_{13}),\ldots,\gamma(\tau_{1N}),\\ & \gamma(\tau_{23}),\gamma(\tau_{24}),\ldots,\gamma(\tau_{2N}),\\ & \vdots\\ & \gamma\left(\tau_{(N-2)(N-1)}\right),\gamma\left(\tau_{(N-2)N}\right),\\ & \gamma\left(\tau_{(N-1)N}\right)\big)\end{aligned}$$

where $\tau_{n_1,n_2} \triangleq \tau_{n_2}-\tau_{n_1}$.

Notice that when $N=2$ all criteria 1), 2), and 3) provide the same result $\Omega_2=(0,\tau_{\min})$, i.e.,

$$\Lambda(\Omega_2)=\begin{bmatrix}1 & \gamma_{\min}\\ \gamma_{\min} & 1\end{bmatrix}$$

independent of the $(E_{\rm a}/N_o)$ value. When $N>2$, different criteria may provide different $\Omega_N$, and the best $\Omega_N$ may depend on the SNR at which the communications' link is operated [28].

## VI. SER Performance

### A. Previous Work

Several authors have calculated the SER performance of UWB in the presence of multipath for both binary and $M$-ary signals, including OPPM, equally correlated PPM, and a hybrid PAM–PPM modulation scheme, using different types of receiver structures (see [7]–[15]).

### B. Error Probability in AWGN

For any value of $M$, the SER $P_e(E_\Psi/N_o,\Gamma_{\rm NO})$ of $N$-OPPM signals is bounded by

$$\begin{aligned}{\rm UB}_e\left(\frac{E_\Psi}{N_o},\Gamma_{\rm NO}\right) &= {\rm UB}_e\left(\frac{E_\Psi}{N_o},\Lambda(\Omega_N)\right)\\ &\quad+(M-N)Q\left(\sqrt{\frac{E_\Psi}{N_o}}\right). \quad (14)\end{aligned}$$

For the particular case $N=2$, we have $L-1$ orthogonal tests and one "pseudoantipodal" test for determining the bound. Hence, the union bound for the symbol error probability is

$$\begin{aligned}{\rm UB}_e\left(\frac{E_\Psi}{N_o},\Gamma_{\rm NO}\right) &= Q\left(\sqrt{\frac{E_\Psi}{N_o}(1-\gamma_{\min})}\right)\\ &\quad+(2L-2)Q\left(\sqrt{\frac{E_\Psi}{N_o}}\right).\end{aligned}$$

To calculate the bit error probability (BER) for $N=2$, we assume that complementary binary patterns representing the data symbols are encoded using a pair of signals consisting of the signal and the pseudoantipodal version of it. If the decoder decides correctly the orthogonal dimension but errs in the pseudoantipodal test, every bit of the word is incorrect. If the decoder decides the wrong orthogonal dimension, bit errors are equally distributed. Hence, the union bound for the BER can be approximated

$$\begin{aligned}{\rm UB}_b\left(\frac{E_\Psi}{N_o},\Gamma_{\rm NO}\right) &\simeq Q\left(\sqrt{\frac{E_\Psi}{N_o}(1-\gamma_{\min})}\right)\\ &\quad+\frac{2L-2}{2}Q\left(\sqrt{\frac{E_\Psi}{N_o}}\right).\end{aligned}$$

### C. Error Probability in Multipath

Performance is calculated by averaging the SER over the multipaths effects, i.e., by taking the expected value $\mathbf{E}_u\{\cdot\}$ over all values of $u_o$

$$\overline{\rm UB}_e\left(\frac{\overline{E}_\Psi}{N_o}\right)=\mathbf{E}_u\left\{{\rm UB}_e\left(\frac{\overline{E}_\Psi\beta^2(u)}{N_o},\Gamma_{\rm NO}(u)\right)\right\} \quad (15)$$

where $(\overline{E}_\Psi/N_o)=\mathbf{E}_u\{\overline{E}_\Psi\beta^2(u)/N_o\}$ is the average received symbol SNR. Calculation of $\overline{\rm UB}_e(\overline{E}_\Psi/N_o)$ in (15) can be approximated by the sample mean value

$$\overline{\rm UB}_e\left(\frac{\overline{E}_\Psi}{N_o}\right)\approx\frac{1}{u_*}\sum_{u_o=1}^{u_*}{\rm UB}_e\left(\frac{\overline{E}_\Psi\beta^2(u_o)}{N_o},\Gamma_{\rm NO}(u_o)\right) \quad (16)$$

computed using an ensemble of UWB pulse responses $\{w(u_o,t)\}$, $u_o=1,2,\ldots,u_*$. More details about this method of performance calculation can be found in [7].

## VII. Channel Capacity

### A. Previous Work

Several authors have calculated the information theoretic channel capacity $C$ for various binary and $M$-ary purely-PPM and hybrid-PPM signals in the presence of AWGN, multiple access interference, and multipath effects (see [12], [14], [15], and the list of references in [32]).

The work in [31] studied $C$ for $M$-ary OPPM signals in AWGN in the context of optical communications. In this section we generalize the capacity calculations in [31] to analyze the case of UWB 2-OPPM signals. In the AWGN channel $C$ depends solely on the SNR. In the multipath channel $C(u_o)$ depends on the SNR $(u_o)$, i.e., depends on both $E_\Psi(u_o)$ and $\alpha(u_o)$, and the averaged capacity is obtained by taking the expected value $\overline{C}\triangleq\mathbf{E}_u\{C(u)\}$ of $C(u_o)$ over the multipath effects [32].

### B. Capacity Calculation in AWGN

Next, we do the capacity calculation for the AWGN channel (please read again the comment on notation at the beginning of Section IV-C).

Consider the model in Fig. 3(c). Since $\overline{\Psi}$ is an invertible function of $\overline{U}$, the observation of $\overline{Y}$ provides an average $I(\overline{Y};\overline{\Psi})$ bits of information about the input $\overline{U}$, where $I(\overline{Y};\overline{\Psi})$ is the mutual information between $\overline{Y}$ and $\overline{\Psi}$. The capacity on the channel is the maximum amount of information that can be transmitted reliably and is given by $C=\max_{p(\overline{\Psi})} I(\overline{Y};\overline{\Psi})$, where $p(\overline{\Psi})$ is the probability distribution of $\overline{\Psi}$.

The channel capacity with input signals that are restricted to a discrete set of $M$ equally likely signals and continuous-valued outputs is given by[11]

$$C=\frac{1}{M}\sum_{\text{all }\overline{\Psi}}\int_{\overline{Y}} p(\overline{Y}|\overline{\Psi})\log_2\left(\frac{p(\overline{Y}|\overline{\Psi})}{\sum_{\text{all }\overline{\Psi}'} p(\overline{Y}|\overline{\Psi}')}\right)d\overline{Y}$$

where $p(\overline{Y}|\overline{\Psi})$ is the pdf of $\overline{Y}$ conditioned on $\overline{\Psi}$. For 2-OPPM signals, this expression can be found to be

$$\begin{aligned}C&=\log_2(M)\\&\quad-\frac{1}{M}\sum_{l=0}^{(M/2)-1}\int_{\overline{Y}} p(\overline{Y}|\overline{\Psi}_{1,l})\log_2\left(\Sigma_{1,1}^{(l)}+\Sigma_{2,1}^{(l)}\right)d\overline{Y}\\&\quad-\frac{1}{M}\sum_{l=0}^{(M/2)-1}\int_{\overline{Y}} p(\overline{Y}|\overline{\Psi}_{2,l})\log_2\left(\Sigma_{1,2}^{(l)}+\Sigma_{2,2}^{(l)}\right)d\overline{Y}\\&=\log_2(M)\\&\quad-\frac{1}{M}\sum_{l=0}^{(M/2)-1}\mathbf{E}_{\overline{Y}|\overline{\Psi}_{1,l}}\left\{\log_2\left(\Sigma_{1,1}^{(l)}+\Sigma_{2,1}^{(l)}\right)\right\}\\&\quad-\frac{1}{M}\sum_{l=0}^{(M/2)-1}\mathbf{E}_{\overline{Y}|\overline{\Psi}_{2,l}}\left\{\log_2\left(\Sigma_{1,2}^{(l)}+\Sigma_{2,2}^{(l)}\right)\right\}\end{aligned}\tag{17}$$

where $p(\overline{Y}|\overline{\Psi}_{n,l})$ is the pdf of $\overline{Y}$ conditioned on $\overline{\Psi}_{n,l}$, $\mathbf{E}_{\overline{Y}|\overline{\Psi}_{n,l}}\{\cdot\}$ is the expected value with respect to $\overline{Y}$ conditioned on $\overline{\Psi}_{n,l}$, and where

$$\Sigma_{n_\mathrm{a},n_b}^{(l)}\triangleq\sum_{l'=0}^{(M/2)-1}\frac{p(\overline{Y}|\overline{\Psi}_{n_\mathrm{a},l'})}{p(\overline{Y}|\overline{\Psi}_{n_b,l})}.$$

To calculate the capacity in (17), we need to specify $p(\overline{Y}|\overline{\Psi}_{n,l})$ for all $\overline{\Psi}_{n,l}$. In our case, the $M$-dimensional vectors $\overline{\Psi}_{n,l}$ have just two components different from zero, i.e., those components with index values $i=2l+1$ and $i=2l+2$ (see example in Table I). By defining $\xi_i\triangleq y_i/\sigma$ and also defining the SNR by $\theta\triangleq 2E_\Psi/N_o$, we find that

$$\begin{aligned}\frac{p(\overline{Y}|\overline{\Psi}_{n_\mathrm{a},l'})}{p(\overline{Y}|\overline{\Psi}_{n_b,l})}=\exp\Big\{&\sqrt{\theta}\psi^{(+)}\left[+\xi_{(2l'+1)}-\xi_{(2l+1)}\right]\\&+\sqrt{\theta}\psi^{(-)}\left[s_\mathrm{a}\xi_{(2l'+2)}-s_b\xi_{(2l+2)}\right]\Big\}\end{aligned}$$

where $s_\mathrm{a}\triangleq(-1)^{(n_\mathrm{a}+1)}$ and $s_b\triangleq(-1)^{(n_b+1)}$, where

$$\begin{aligned}&\xi_{2l+1},\xi_{2l'+1}, &&\text{each has pdf } N(\sqrt{\theta}\psi^{(+)},1)\\&\xi_{2l+2},\xi_{2l'+2}, &&\text{each has pdf } N(\pm\sqrt{\theta}\psi^{(-)},1)\\&\xi_i, i\neq 2l+1,2l+2, &&\text{each has pdf } N(0,1)\end{aligned}$$

and where $N(\cdot,\cdot)$ represents the normal distribution. Hence

$$\begin{aligned}\sum\nolimits_{n_\mathrm{a},n_b}^{(l)}=\sum_{l'=0}^{(M/2)-1}\exp\Big\{&\sqrt{\theta}\psi^{(+)}\left[+\xi_{(2l'+1)}-\xi_{(2l+1)}\right]\\&+\sqrt{\theta}\psi^{(-)}\left[(-1)^{(n_\mathrm{a}+1)}\xi_{(2l'+2)}-(-1)^{(n_b+1)}\xi_{(2l+2)}\right]\Big\}.\end{aligned}$$

To calculate the capacity in (17), we need to calculate the $M$-dimensional expectations $\mathbf{E}_{\overline{Y}|\overline{\Psi}_{n,l}}\{\cdot\}$. To find a close form solution for these $M$-dimensional expectations is a difficult task. These expectations can be calculated using numerical methods. They also can be estimated via Monte Carlo simulation [31]. The method is to generate pseudorandom $M$-vectors $\overline{Y}$ according to the probability density $p(\overline{Y}|\overline{\Psi}_{n,l})$. For each generated sample $\overline{Y}$, the function inside the logarithm is evaluated. Finally, the sample average of the logarithm is calculated.

Notice that by using $\tau=\tau_{\min}$, then (17) is the capacity of 2-OPPM, and that if we use $\tau=T_w$, then (17) becomes the capacity of OPPM.

### C. Averaged Channel Capacity for Multipath Case

To find $C(u_o)$, we add the index $u_o$ to (17), i.e., we use $\overline{Y}(u_o)$, $\overline{\Psi}_{n,l}(u_o)$, $\psi^{(+)}(u_o)$, $\psi^{(-)}(u_o)$, $\Sigma_{n_\mathrm{a},n_b}^{(l)}(u_o)$, $\xi(u_o)$, and $\theta(u_o)$. Clearly, the multipath effects change for different $u_o$ and, therefore, $E_\Psi(u_o)$ and $\alpha(u_o)$ (and all the quantities in the previous list) change with $u_o$ [30], [32]. Hence, to calculate the average capacity $\overline{C}$, we need to calculate the expectation $\mathbf{E}_u\{\cdot\}$. This expectation can also be estimated via Monte Carlo simulations using the sample mean value

$$\overline{C}\approx\frac{1}{u_*}\sum_{u_o=1}^{u_*}C(u_o)\tag{18}$$

computed using an ensemble of UWB pulse responses $\{w(u_o,t)\}$, $u_o=1,2,\ldots,u_*$.

[11]Capacity calculations involve an optimization step over the input distribution. Because of the symmetry of orthogonal signals and of the channel considered, capacity is achieved with an equiprobable $M$-ary source distribution [31]. In the case of 2-OPPM, we can reason that the two signals in each orthogonal subset are symmetrical; therefore, they are conditionally equally likely. Giving a preference to a particular pair of signals would reduce the $M$-ary throughput, and hence, all the orthogonal subsets are also symmetrical; therefore, they are conditionally equally likely. Hence, we can conjecture that for the 2-OPPM case, capacity is also achieved with an equiprobable $M$-ary source distribution. Since we are not giving a formal proof here, we can think of $C$ as an achievable rate using equally likely signals.

## VIII. Signal Design and PSD Calculation Example

### A. Signal Design for Gaussian Pulse

In this example, the UWB pulse is the second derivative of a Gaussian pulse

$$w(t) = \left[1 - 4\pi\left[\frac{t}{t_n}\right]^2\right]\exp\left(-2\pi\left[\frac{t}{t_n}\right]^2\right) \tag{19}$$

for $-T_w/2 \le t \le T_w/2$, where $t_n$ is a parameter that determines the pulse duration, with energy $E_w = 3t_n/8$. The signal correlation function is

$$\gamma(\tau) = \left[1 - 4\pi\left[\frac{\tau}{t_n}\right]^2 + \frac{4\pi^2}{3}\left[\frac{\tau}{t_n}\right]^4\right] \times \exp\left(-\pi\left[\frac{\tau}{t_n}\right]^2\right)$$

for $-T_w \le \tau \le T_w$, with $\gamma_{\min} \simeq -0.6181$ for any value of $t_n$. The value of $\tau_{\min}$ depends on $T_w$ (i.e., depends on $t_n$).

When $t_n = 0.7531$ ns, we get a pulse duration $T_w \simeq 2.0$ ns and $\tau_{\min} \simeq 0.4068$ ns. In this case, the spectrum of $w(t)$ is centered at 1.1 GHz, with a 3-dB bandwidth of about 1.2 GHz, easily satisfying the traditional definition of UWB signal stating that the 10-dB bandwidth of the signal should be at least 20% of its center frequency [33]. The optimization criterion 2) was applied using a computer program with a simplex search method [34]. Table II shows the results for $N = 4$.

### B. Signal PSD for Gaussian Pulse

Using the pulse in (19) to calculate $F_w(f)$ in (6) gives

$$|F_w(f)| = \sqrt{2}t_n\left(\frac{\pi(ft_n)^2}{2}\right) \times \exp\left(-\frac{\pi(ft_n)^2}{2}\right)$$

with a maximum at $f_{\rm m} = 1/t_n\sqrt{2/\pi}$. Fig. 4 shows PSD calculations using (6) for $P_i = 1/M$, $M = 8$, $N = 2$, $L = M/N = 4$, $T_o = T_w + \tau_{\min} = 2.4086$ ns, $T_f = 12$ ns, and $N_s = 11$. Fig. 4 also shows the effect of the TH code on the PSD for one particular TH-code realization.

### C. Signal Design for Gated Sine Wave

The UWB pulse considered in this example is based on a gated sine wave

$$w(t) = \sin\left(2\pi\frac{Q}{T_w}t\right) \tag{20}$$

for $-T_w/2 \le t \le T_w/2$, where $Q$ is a positive integer, with energy $E_w = (T_w/2)$. The signal correlation function is

$$\gamma(\tau) = \frac{1}{E_w}\frac{T_w - |\tau|}{T_w}\cos\left(2\pi\frac{Q}{T_w}\tau\right)$$

for $-T_w \le \tau \le T_w$, with $\gamma_{\min} \simeq -0.9501$ for $Q = 10$ and any value of $T_w$. The value of $\tau_{\min}$ depends on both $Q$ and $T_w$.

When $T_w = 2.0$ ns and $Q = 10$, we have $\tau_{\min} \simeq 0.0995$ ns. In this case, the spectrum of $w(t)$ is centered at $Q/T_w = 5$ GHz, with a 3-dB bandwidth of about 500 MHz, easily satisfying the new definition of UWB signal stating that the 10-dB bandwidth of the signal should be at least 500 MHz [33]. The optimization criterion 3) was calculated using a computer program. Table III shows the results for $N = 3$.

### D. Signal PSD for Gated Sine Wave

Using the pulse in (20) to calculate $F_w(f)$ in (6) gives

$$|F_w(f)| = T_w{\rm sinc}\left(\pi T_w\left(f - \frac{Q}{T_w}\right)\right)$$

with a maximum at $f_{\rm m} = Q/T_w$. Fig. 5 shows PSD calculations using (6) for $P_i = 1/M$, $M = 6$, $N = 2$, $L = M/N = 3$, $T_o = T_w + \tau_{\min} = 2.0995$ ns, $T_f = 12$ ns and $N_s = 11$. Fig. 5 also shows the effect of the TH code on the PSD for one particular TH-code realization.

## IX. SER Example

### A. SER in AWGN for Gaussian Pulse

Performance for different values $(E_\Psi/N_o)$ is calculated utilizing the optimized time shift $\Omega_N$ corresponding to that $(E_\Psi/N_o)$ value (see Table II). Fig. 6(a) shows ${\rm UB}_e(E_\Psi/N_o, \Gamma_{\rm NO})$ and ${\rm UB}_e(E_\Psi/N_o, \Gamma_{\rm OR})$ in (14) for different $N$, $L$, and $M$.

### B. SER in Multipath for Gaussian Pulse

To characterize the multipath channel in this case, we use an ensemble formed with experimental channel pulse responses $w(u_o, t)$ measured in different rooms of an office building.[12]

A total of $u_* = 294$ channel pulse responses $w(u_o, t)$ are used (49 for each different room, a total of six rooms). The measured $w(u_o, t)$ has $T_{\rm a} \simeq 300$ ns. By selecting $T_f = 500$ ns, we make sure that $T_f > T_{\rm a} + LT_o$.[13] The set of $u_*$ values is used to compute an equal number of $E_\Psi(u_o)$, $\alpha^2(u_o)$, $\Gamma_{\rm NO}(u_o)$, and $\Gamma_{\rm OR}(u_o)$ using the method described in [7].

Fig. 6(b) shows the averaged SER $\mathbf{E}_u\{{\rm UB}_e(\overline{E}_\Psi\beta^2(u)/N_o, \Gamma_{\rm NO}(u))\}$ and $\mathbf{E}_u\{{\rm UB}_e(\overline{E}_\Psi\beta^2(u)/N_o, \Gamma_{\rm OR}(u))\}$ in (16) for different $N$, $L$, and $M$. For every value of $(E_\Psi/N_o)$, the same $\Omega_N$ value corresponding to $(\overline{E}_\Psi/N_o) = 12$ dB in Table II is used.

### C. SER in AWGN for Gated Sine Wave

Performance in AWGN is calculated with the optimized time shift $\Omega_N$ (see Table III). Fig. 7(a) shows ${\rm UB}_e(E_\Psi/N_o, \Gamma_{\rm NO})$, and ${\rm UB}_e(E_\Psi/N_o, \Gamma_{\rm OR})$ in (14) for different $N$, $L$, and $M$.

### D. SER in Multipath for Gated Sine Wave

To characterize the multipath channel in this case, we use an autoregressive channel model [35], [36] to form and ensemble

[12]These UWB pulses are taken from the Time Domain Corporation Indoor Channel Database, which is available at USC's ULTRA-LAB WEB site at http://click.usc.edu/New-Site/database.html.

[13]For consistency, we use the same $T_f$ in both Gaussian and multipath channels and for both pulse shapes considered here.

TABLE II
OPTIMIZED VALUES $\Omega_N$, $\Lambda(\Omega_N)$, AND $\mathrm{UB}_e(E_a/N_o, \Lambda(\Omega_N))$ FOR $N = 4$ AND DIFFERENT $(E_a/N_o)$ CALCULATED USING THE GAUSSIAN PULSE IN (19)

| $\left(\frac{E_a}{N_o}\right)$ (dB) | $\Omega_4=(\tau_1,\tau_2,\tau_3,\tau_4)$ (ns) | $\{\lambda_{21}, \lambda_{31}, \lambda_{41}, \lambda_{32}, \lambda_{42}, \lambda_{43}\} \in \Lambda(\Omega_4)$ | $\mathrm{UB}_e\left(\frac{E_a}{N_o}, \Lambda(\Omega_4)\right)$ (prob. of error) |
|---|---|---|---|
| 2 | (0.0000,0.3264,0.5945,0.9209) | {−0.4967,−0.2429,0.1061,−0.2561,−0.2429,−0.4967} | $2.4003952e^{-1}$ |
| 4 | (0.0000,0.3211,0.5902,0.9113) | {−0.4800,−0.2548,0.1087,−0.2608,−0.2548,−0.4800} | $1.1726925e^{-1}$ |
| 6 | (0.0000,0.3153,0.5862,0.9015) | {−0.4604,−0.2659,0.1111,−0.2698,−0.2659,−0.4604} | $4.1460574e^{-2}$ |
| 8 | (0.000,0.3109,0.5842,0.8951) | {−0.4445,−0.2714,0.1124,−0.2821,−0.2714,−0.4445} | $9.1811626e^{-3}$ |
| 10 | (0.0000,0.3211,0.5966,0.9178) | {−0.4799,−0.2372,0.1070,−0.2929,−0.2370,−0.4801} | $1.0597741e^{-3}$ |
| 12 | (0.0000,0.2536,0.5058,0.7594) | {−0.1790,−0.4827,0.0749,−0.1714,−0.4826,−0.1790} | $4.4588128e^{-5}$ |
| 14 | (0.0000,0.2452,0.4901,0.7352) | {−0.1319,−0.5186,0.0489,−0.1304,−0.5187,−0.1317} | $3.2869771e^{-7}$ |
| 16 | (0.0000,0.2452,0.4901,0.7352) | {−0.1049,−0.5378,0.0306,−0.1045,−0.5379,−0.1046} | $1.55400285e^{-10}$ |
| 18 | (0.0000,0.2374,0.4746,0.7119) | {−0.0867,−0.5500,0.0168,−0.0858,−0.5501,−0.0866} | $9.3470225e^{-16}$ |

TABLE III
OPTIMIZED VALUES OF $\Omega_N$ AND $\Lambda(\Omega_N)$ FOR $N = 3$, AND VALUES OF $\tau_{\min}$, $\gamma_{\min}$, AND SNR ADVANTAGE $10\log_{10}(1-\gamma_{\min})$. VALUES ARE CALCULATED USING THE GATED SINE WAVE IN (20) WITH $Q = 1, 2, 3, 4, 10$

| $Q$ | $\Omega_3=(\tau_1,\tau_2,\tau_3)$ | $\{\lambda_{21}, \lambda_{31}, \lambda_{32}\} \in \Lambda(\Omega_3)$ (ns) | $\gamma(\tau_{\min})=\gamma_{\min}$ | $10\log_{10}(1-\gamma_{\min})$ (dB) |
|---|---|---|---|---|
| 1 | (0.00,0.62,1.24) | {−0.2540,−0.2770,−0.2540} | $\gamma(0.91)=-0.5234$ | 1.8 |
| 2 | (0.00,0.33,0.66) | {−0.4023,−0.3594,−0.4023} | $\gamma(0.48)=-0.7540$ | 2.4 |
| 3 | (0.00,0.22,0.44) | {−0.4288,−0.4179,−0.4288} | $\gamma(0.33)=-0.8346$ | 2.6 |
| 4 | (0.00,0.16,0.32) | {−0.3917,−0.5354,−0.3917} | $\gamma(0.25)=-0.8750$ | 2.7 |
| 10 | (0.00,0.06,0.12) | {−0.2997,−0.7605,−0.2997} | $\gamma(0.1)=-0.9500$ | 2.7 |

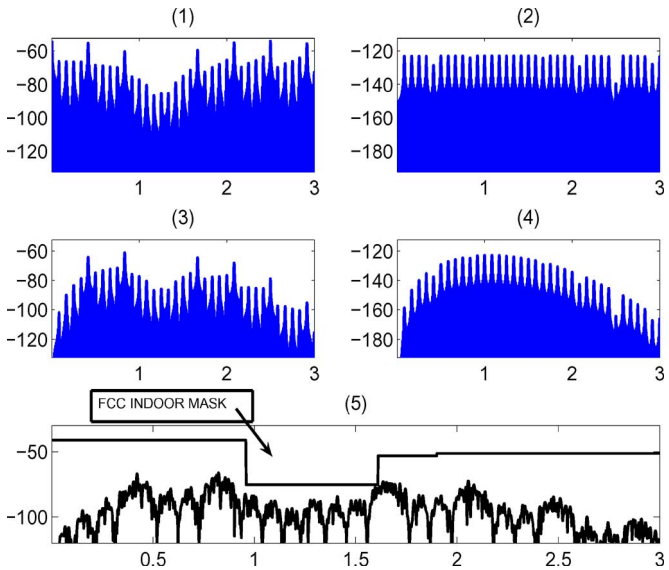


Fig. 4. Subplots (1)–(2) show $\mathrm{PSD}_d(f)/T_f^2$ and $\mathrm{PSD}_c(f)/T_f$, respectively. Subplots (3)–(4) show $(|F_w(f)|^2\mathrm{PSD}_d(f))/T_s^2$ and $(|F_w(f)|^2\mathrm{PSD}_c(f))/T_s$, respectively. Subplot (5) shows $\mathrm{PSD}(f)$ including the effect of a random TH code with maximum time shift $(Tf/2)$. Plots are for the Gaussian pulse in (19).

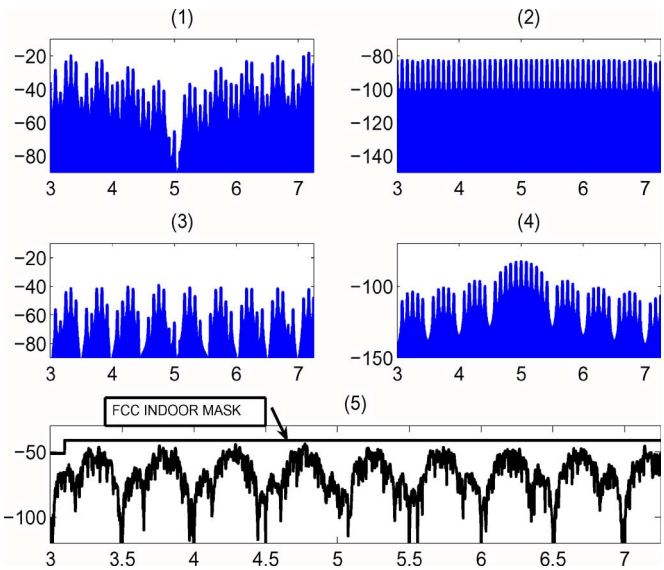


Fig. 5. Subplots (1)–(2) show $\mathrm{PSD}_d(f)/T_f^2$ and $\mathrm{PSD}_c(f)/T_f$, respectively. Subplots (3)–(4) show $|F_w(f)|^2\mathrm{PSD}_d(f)/T_s^2$ and $|F_w(f)|^2\mathrm{PSD}_c(f)/T_s$, respectively. Subplot (5) shows $\mathrm{PSD}(f)$ including the effect of a random TH code with maximum time shift $(Tf/2)$. Plots are for the gated sine wave in (20) with $Q = 10$.

of modeled channel pulse responses $w(u_o, t)$ characterizing different rooms in a variety of houses. We consider line-of-sight (LOS) scenarios with $D = 3, 6$, and 9 m and non-LOS (NLOS) scenarios with $D = 1, 2$, and 3 m (results are averaged over the different values of $D$).

A total of $u_* = 294$ channel pulse responses $w(u_o, t)$ are used (49 per each distance value). The simulated $w(u_o, t)$ has $T_a \simeq 160$ ns. The set of $u_*$ pulse responses is used to calculate an equal number of random values $E_\Psi(u_o)$, $\alpha^2(u_o)$, $\Gamma_{\mathrm{NO}}(u_o)$, and $\Gamma_{\mathrm{OR}}(u_o)$ using the method described in [37].

Fig. 7(b) shows the averaged SER $\mathbf{E}_u\{\mathrm{UB}_e(\overline{E}_\Psi\beta^2(u)/N_o, \Gamma_{\mathrm{NO}}(u))\}$ and $\mathbf{E}_u\{\mathrm{UB}_e(\overline{E}_\Psi\beta^2(u)/N_o, \Gamma_{\mathrm{OR}}(u))\}$ in (16) for different $N$, $L$, and $M$. For every value of $(\overline{E}_\Psi/N_o)$, the same optimized $\Omega_N$ value is used.

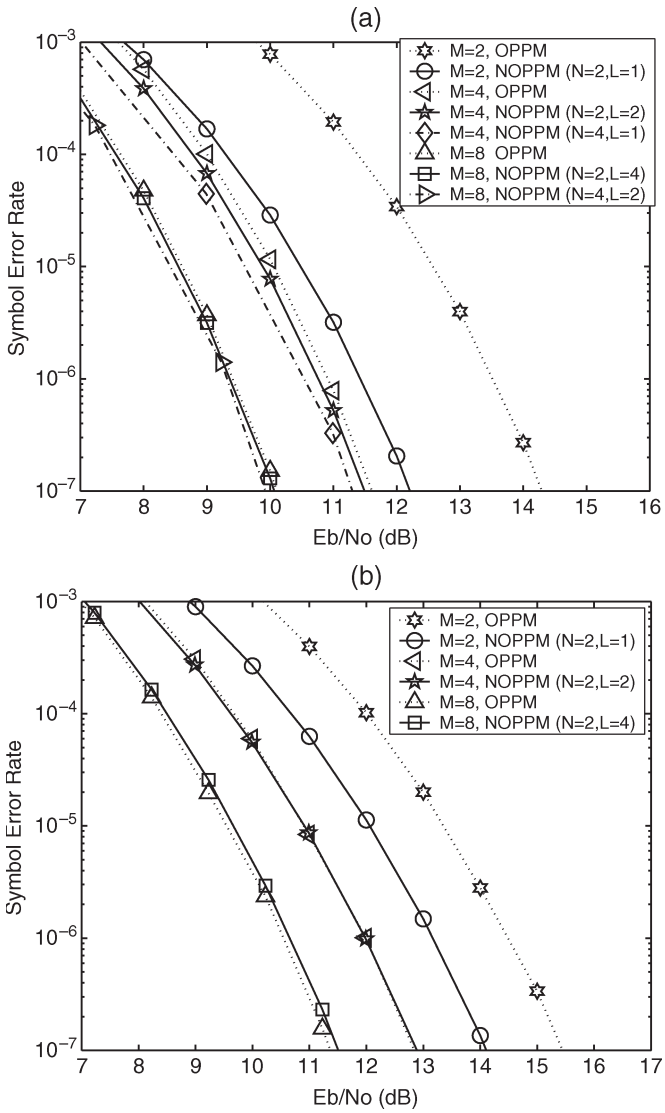


Fig. 6. SER for $N$-OPPM versus OPPM, for $M = 2, 4, 8$; $N = 2, 4$; $L = 1, 2, 4$. (a) AWGN channel. (b) Multipath channel (Time Domain database). The UWB pulse is the second derivative of a Gaussian pulse in (19).


Fig. 7. SER for $N$-OPPM versus OPPM with $M = 3, 6$; $N = 3$; $L = 1, 2$. (a) AWGN channel. (b) Multipath channel (AR model). The UWB pulse is the pulsed sine wave in (20) with $Q = 1, 10$.

### E. Summary of SER Results

Table IV summarizes the SER results for different values of $M$.

TABLE IV
SNR ADVANTAGE OF $N$-OPPM SIGNALS OVER OPPM SIGNALS, CALCULATED FOR DIFFERENT $M$, IN AWGN AND MULTIPATH CHANNELS, FOR BOTH UWB PULSES

| | Gaussian pulse | Gaussian pulse | Sine pulse $Q = 10$ | Sine pulse $Q = 10$ |
|---|---|---|---|---|
| $M$ | SNR gain (dB) (AWGN) | SNR gain (dB) (Multipath) | SNR gain (dB) (AWGN) | SNR gain (dB) (Multipath) |
| 2 | 2.09 | 1.30 | 2.90 | - |
| 3 | - | - | 1.31 | 1.78 |
| 4 | 0.25 | 0.0 | - | - |
| 6 | - | - | 0.16 | 0.24 |
| 8 | 0.05 | -0.2 | - | - |

## X. CAPACITY CALCULATION EXAMPLE

### A. Results in AWGN

The capacity $C$ is calculated using (17) and Monte Carlo simulation. Fig. 8 shows $C$ versus $E_b/N_o \triangleq (2E_\Psi/N_o)/2C$ for Gaussian and gated sine wave UWB pulses, using $M = 2, 4, 8$.

### B. Results in Multipath

For capacity in multipath channels, the set of $u_*$ random values is used to compute (18) by Monte Carlo simulation. Fig. 9 show $\overline{C}$ versus $\overline{E}_b/N_o \triangleq (2\overline{E}_\Psi/N_o)/2\overline{C}$ for the gated sine wave pulse, using $M = 2$ for both AWGN and multipath channels.

### C. Summary of Capacity Results

Table V summarizes the $C$ results for different values of $M$.

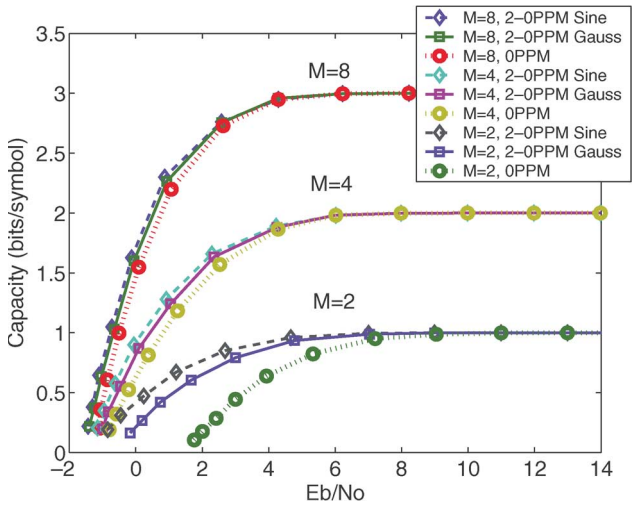


Fig. 8. Channel-capacity results in AWGN for 2-OPPM signals versus OPPM signals using the Gaussian and the gated sine wave pulses.

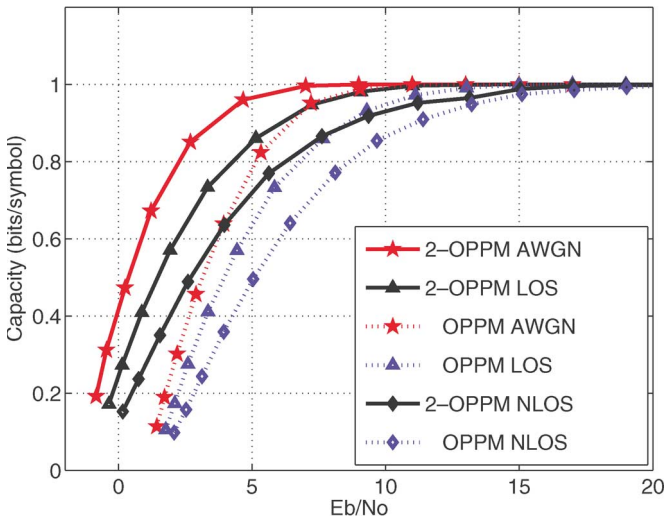


Fig. 9. Channel-capacity results for AWGN and multipath (LOS and NLOS) channels for $M = 2$ using the gated sine wave pulse and the AR multipath channel model.

TABLE V
APPROXIMATE SNR ADVANTAGE OF 2-OPPM SIGNALS OVER OPPM SIGNALS TO ACHIEVE 90% OF THE CAPACITY, CALCULATED FOR DIFFERENT $M$ USING BOTH UWB PULSES

| | Gaussian pulse | Sine pulse $Q = 10$ | Sine pulse $Q = 10$ |
|---|---|---|---|
| $M$ | SNR gain (dB) (AWGN) | SNR gain (dB) (AWGN) | SNR gain (dB) (Multipath) |
| 2 | 2.1 | 2.7 | 2.5 |
| 4 | 0.5 | 0.5 | - |
| 8 | 0.1 | 0.1 | - |

## XI. DISCUSSION AND CONCLUSION

This paper presents a multidimensional spherical signal design for $M$-ary UWB communications using PPM. The pulse positions are numerically optimized to get signals with favorable correlation properties. Three optimality criteria for the pulse positions are presented for the AWGN channel (in this paper, we do not optimize in multipath channels).

The $M$-ary PPM signals are linearly independent and have $N$-orthogonal correlation properties. The number $N$ of signals that is negatively correlated reaches a limit as $N$ grows. Since signals are either orthogonal or negatively correlated, they require coherent detection.

The $N$-OPPM signals can accommodate a larger value of $M$ than OPPM signals for constant frame size and pulsewidth, allowing to increase the symbol transmission rate or the use of error correcting codes. However, the $M$-ary receiver requires $N$ correlators for $N$-OPPM signals, while OPPM signals requires 1 correlator.

We calculated the PSD of $N$-OPPM as a function of both the $M$-ary PPM time-shift pattern and the shape of the UWB pulse. Results shows that the PPM time-shift pattern can be manipulated to shape the PSD and decrease the level of the discrete components. However, this PPM manipulation changes the $N$-OPPM correlation properties and can impact the performance of the signal set.

We studied the time-shift-coherent communications using a kind of Rake receiver that is perfectly matched to the received signals and perfectly synchronized with the transmitter. We analyzed both the SER and $C$ of $N$-OPPM for a single-link UWB communications over both AWGN and multipath channels. For multipath we took into account random variations in both energy and correlation values.

The numerical results confirm that for low values of $M$, the $N$-OPPM has lower SER and higher $C$ than OPPM for the same SNR, and that for larger values of $M$, it achieves similar SER and $C$. Hence, for low $M$, the $N$-OPPM signals have an SNR advantage over the OPPM signals in the sense that they achieve $C$ and SER at lower SNR. In the $N$-OPPM case, the SNR advantage decreases as $M$ increases because more signals that are pair-wise orthogonal are added to the $N$-OPPM signal set. With different pulse shapes, we can get different SNR advantages, and we can also have different sensitivity to synchronization errors.

For a given set of correlation values, the SNR advantage in AWGN is maintained from low SNR to high SNR values. This is expected, since the negative correlation values translate to better signal distance properties, which can be viewed as an SNR enhancement in AWGN. This is not the case in multipath channels because fading affects more the low SNR region of the curve with higher slope.

The fading margin is the increase in signal power required to preserve performance on fading versus nonfading conditions (notice that fading margin in the UWB AR model is much larger than in the time domain UWB pulse database). From the results, we can see that SER has bigger fading margin than $C$. This can be explained considering that $C$ is the expected value of the logarithm of a function of the SNR; hence, the $C$ has a smoother variation with respect to SNR than the SER.

We emphasize that the motivation of this paper is not just the SNR gain but the tradeoff between transmission rate, signal performance, and receiver complexity.

The performance results for the AWGN channel are generic since the pulse duration $T_w$ was not involved in the derivation. These results are also independent of $N_s$.

The performance results in the presence of multipath took into account the UWB multipath resolution capability, considering the statistical properties of both the random variations of the energy and correlation values. By assuming that the frame period $T_f$ is large enough, both interpulse and intersymbol interference can be neglected, and the results become independent of the value of $N_s$. In this case, the Rake receiver is matched to the individual received "pulse." If we allow interpulse interference (or if the channel is not slowly varying), then we can still use the simplified analysis, but the receiver would need to be matched to the whole received signal, and ISI could be neglected if we use a large number of "pulses" per symbol.

For performance results in a multiple-user environment, the use of $M$-ary signals allows to reduce the required transmitter power maintaining the number of users, the data transmission rate, and the multiple access performance. The bit energy $E_b$ to achieve SER at a certain distance is limited by the symbol rate $R_s$, and the average power in PSD. To decrease SER using $M$-ary modulation, we need to maintain $E_b/N_o$ as $M$ grows by either increasing the signal power or reducing $R_s$. Due to PSD limitations, the second approach is preferred, since using a smaller $R_s$ increases the processing gain.

For future work, capacity results in the presence of multiple-user interference will need to take into account both the processing gain capability of UWB (which is a function of $T_s = N_s T_f$ and $T_w$) and the pdf of the UWB interference.

## ACKNOWLEDGMENT

The author would like to thank the anonymous reviewers for their constructive comments and insights that helped improve this paper.

## REFERENCES

[1] R. A. Scholtz, "Multiple access with time hopping impulse modulation," in *Proc. IEEE MILCOM Conf.*, 1993, pp. 447–450.

[2] F. Ramírez-Mireles and R. A. Scholtz, "System performance of impulse radio modulation," in *Proc. IEEE RAWCON Conf.*, Aug. 1998, pp. 67–70.

[3] "Special issue on ultra-wideband radio in multiaccess wireless communications," *IEEE J. Sel. Areas Commun.*, vol. 20, no. 9, Dec. 2002.

[4] S. Roy, J. R. Foerster, V. S. Somayazulu, and D. G. Leeper, "Ultra-wideband radio design: The promise of high-speed, short-range wireless connectivity," Invited Paper, *Proc. IEEE*, vol. 92, no. 2, pp. 295–311, Feb. 2004.

[5] R. C. Qiu, H. Liu, and X. Shen, "Ultra-wideband for multiple access communications," *IEEE Commun. Mag.*, vol. 43, no. 2, pp. 2–8, Feb. 2005.

[6] A. F. Molisch *et al.*, "Mitsubishi electrics time-hopping impulse radio standards proposal," *IEEE P802.15 Working Group for Wireless Personal Area Networks (WPANs), Contribution IEEE P802.15-03113*, May 2003.

[7] F. Ramírez-Mireles, "On performance of ultra wideband signals in Gaussian noise and dense multipath," *IEEE Trans. Veh. Technol.*, vol. 50, no. 1, pp. 244–249, Jan. 2001.

[8] F. Ramírez-Mireles, "Performance of ultrawideband SSMA using time hopping and $M$-ary PPM," *IEEE J. Sel. Areas Commun.*, vol. 19, no. 6, pp. 1186–1196, Jun. 2001.

[9] F. Ramírez-Mireles, "Error probability of ultra wideband SSMA in a dense multipath environment," in *Proc. IEEE MILCOM Conf.*, Oct. 2002, pp. 1081–1084.

[10] L. Yang and G. B. Giannakis, "Impulse radio multiple access through ISI channels with multi-stage block-spreading," in *Proc. IEEE UWBST Conf.*, May 2002, pp. 277–282.

[11] G. Durisi *et al.*, "A general method for error probability computation of UWB systems for indoor multiuser communications," *J. Commun. Netw.*, vol. 5, no. 4, pp. 354–364, Dec. 2003.

[12] L. Zhao and A. M. Haimovich, "Capacity of $M$-ary PPM ultra-wideband communications over AWGN channels," in *Proc. IEEE Veh. Technol. Conf.*, Oct. 2001, pp. 1191–1195.

[13] L. Zhao and A. M. Haimovich, "The capacity of an UWB multiple-access communications system," in *Proc. IEEE Int. Commun. Conf.*, 2002, pp. 1964–1968.

[14] J. Zhang, R. A. Kennedy, and T. D. Abhayapala, "New results on the capacity of $M$-ary PPM ultra-wideband systems," in *Proc. IEEE Int. Conf. Commun.*, May 2003, pp. 2867–2871.

[15] R. Pasand, S. Khaleshosseini, J. Nielsen, and A. Sesay, "The capacity of asynchronous $M$-ary time hopping PPM UWB multiple access communication systems," in *Proc. IEEE Veh. Technol. Conf.*, Sep. 2004, pp. 4745–4749.

[16] F. Ramírez-Mireles, "UWB $M$-ary $N$-orthogonal PPM signals in AWGN and multipath channels," in *Proc. IEEE Veh. Technol. Conf.*, Oct. 2004, pp. 5255–5259.

[17] F. Ramírez-Mireles, "Capacity of UWB $M$-ary 2-orthogonal PPM signals in AWGN and multipath channels," in *Proc. IEEE 39th Annu. Asilomar Conf. Signals, Syst., and Comput.*, Nov. 2005, pp. 976–980.

[18] R. Gagliardi, J. Robbins, and H. Taylor, "Acquisition sequences in PPM communications," *IEEE Trans. Inf. Theory*, vol. IT-33, no. 5, pp. 738–744, Sep. 1987.

[19] C. N. Georghiades, "On PPM sequences with good autocorrelation properties," *IEEE Trans. Inf. Theory*, vol. 34, no. 3, pp. 571–576, May 1988.

[20] S. W. Golomb, "Construction of signals with favourable correlation properties," in *Surveys in Combinatorics*, ser. London Mathematical Society Lecture Notes Series 166. Cambridge, U.K.: Cambridge Univ. Press, 1991.

[21] R. M. Gagliardi, *Introduction to Telecommunications Engineering*. New York: Wiley, 1988, pp. 357–437.

[22] I. S. Reed and R. A. Scholtz, "$N$-orthogonal phase-modulated codes," *IEEE Trans. Inf. Theory*, vol. IT-12, no. 3, pp. 388–395, Jul. 1966.

[23] A. J. Viterbi and J. J. Stiffler, "Performance of $N$-orthogonal codes," *IEEE Trans. Inf. Theory*, vol. IT-13, no. 3, pp. 521–522, Jul. 1967.

[24] F. Ramírez-Mireles and R. A. Scholtz, "$N$-orthogonal PPM signals for ultra wide bandwidth impulse radio modulation," in *Proc. IEEE Commun. Theory Miniconf.*, Nov. 1997, pp. 6–11.

[25] M. K. Simon, S. M. Hinedi, and W. C. Lindsey, *Digital Communications Techniques: Signal Design and Detection*. New York: Prentice-Hall, 1995, pp. 63–68.

[26] A. Papoulis, *Signal Analysis*. Singapore: McGraw-Hill, 1984, pp. 68–72.

[27] J. G. Proakis, *Digital Communications*. New York: McGraw-Hill, 1995, pp. 797–806.

[28] C. L. Weber, *Elements of Detection and Signal Design*. New York: Springer-Verlag, 1987.

[29] M. J. Steiner, "Contributions to statistical communication Theory," Ph.D. dissertation, Dept. Electr. Eng., Univ. Maryland, College Park, 1994.

[30] F. Ramírez-Mireles, "Signal design for ultra wideband communications in dense multipath," *IEEE Trans. Veh. Technol.*, vol. 51, no. 6, pp. 1517–1521, Nov. 2002.

[31] S. Dolinar, D. Divsalar, J. Hamkins, and F. Pollara, "Capacity of pulse-position modulation (PPM) on Gaussian and Webb channels," *JPL TMO Progress Report*, vol. 42–142, pp. 1–31, Apr.–Jun. 2000.

[32] F. Ramírez-Mireles, "On the capacity of UWB over multipath channels," *IEEE Commun. Lett.*, vol. 9, no. 6, pp. 523–525, Jun. 2005.

[33] FCC, released, ET Docket 98-153, FCC 02-48, *First Report and Order in the Matter of Revision of Part 15 of the Commission's Rules Regarding Ultra-Wideband Transmission Systems*, Apr. 22, 2002.

[34] J. C. Lagarias, J. A. Reeds, M. H. Wright, and P. E. Wright, "Convergence properties of the Nelder–Mead simplex algorithm in low dimensions," in *SIAM J. Optim.*, Dec. 1998, pp. 112–147.

[35] W. Turin, R. Jana, S. Ghassemzadeh, C. Rice, and V. Tarokh, "Autoregressive modeling of an indoor UWB channel," in *Proc. Dig. Papers UWBST' Conf.*, May 2002, pp. 71–74.

[36] S. Ghassemzadeh, R. Jana, C. Rice, W. Turin, and V. Tarokh, "A statistical path loss model for in-home UWB channel," in *Proc. Dig. Papers UWBST Conf.*, May 2002, pp. 59–64.

[37] R. Bastidas-Puga, F. Ramírez-Mireles, and D. Muñoz-Rodríguez, "On fading margin in ultrawideband communications over multipath channels," *IEEE Trans. Broadcast.*, vol. 51, no. 3, pp. 366–370, Sep. 2005.

**Fernando Ramírez-Mireles** (M'88–SM'01) received the B.S.E.E. degree from Metropolitan Autonomous University (UAM), México, México, the M.S. degree in electrical engineering from Center for Advanced Studies of IPN (CINVESTAV), México, and the Ph.D. degree in electrical engineering from University of Southern California (USC), Los Angeles.

From 1988 to 1992, he worked and/or consulted for CINVESTAV, UAM, the Mexican Telephone Company, and the National Bank of México. From 1996 to 1998, he was a Research Assistant at USC's Communication Sciences Institute working on UWB communications. From 1997 to 2003, he worked as a Systems Engineer at Torrey Science Corporation, San Diego, CA, on spread spectrum LEO satellite Communications, at Glenayre Technologies, Santa Clara, CA, on definition of demodulation architectures for Narrowband Personal Communications Services mobile terminals; at Aware, Inc., Lafayette, CA, on technology development for digital subscriber line (DSL) standards; and at Ikanos Communications, Fremont, CA, where he worked on system design and algorithm development for VDSL. Currently, he is a Full Professor in the Digital Systems Department, Instituto Tecnológico Autónomo de México, México City, where he lectures on communications systems. He has coauthored three IEC comprehensive technology reports and over 30 technical articles in areas including UWB, DSL, and speech recognition. His work on UWB is frequently cited, and he is the holder of four patents on ADSL and VDSL with two more pending. He was in the Technical Program Committee of IFIP ICPWC2006, ICPWC2207, and WPMC 2006, and he acts as a Reviewer for transactions and conferences. He was a Coordinator at the first and second French-Mexican Summer Schools in Telecommunications held in México and France, and he has been an Invited Speaker at professional meetings. His research interests include UWB communications (modulation and signal design, performance in multipath channels) and DSL (synchronization and crosstalk interference).

Dr. Ramírez-Mireles is a member of the National System of Researchers SNI (México). He is listed in Marquis *Who's Who in America* and in *International Who's Who of Professionals*. He was a Fulbright Scholar while studying his Ph.D. program at USC. In México, he received an Honorific Mention in the IV Ericsson's National Prize of Science and Technology, and received the Medal to the Universitarian Merit. He was selected twice by the committee of the Best Students of México Award. He is a member of Tau Beta Pi and the Society of Hispanic Professional Engineers.